



Supersonic Inlet Test for a Quiet Supersonic Transport Technology Demonstrator in the NASA Glenn 8- by 6-Foot Supersonic Wind Tunnel

*Raymond Castner and Stephanie Simerly
Glenn Research Center, Cleveland, Ohio*

*Michael Rankin
Lockheed Martin, Palmdale, California*

NASA STI Program . . . in Profile

Since its founding, NASA has been dedicated to the advancement of aeronautics and space science. The NASA Scientific and Technical Information (STI) Program plays a key part in helping NASA maintain this important role.

The NASA STI Program operates under the auspices of the Agency Chief Information Officer. It collects, organizes, provides for archiving, and disseminates NASA's STI. The NASA STI Program provides access to the NASA Technical Report Server—Registered (NTRS Reg) and NASA Technical Report Server—Public (NTRS) thus providing one of the largest collections of aeronautical and space science STI in the world. Results are published in both non-NASA channels and by NASA in the NASA STI Report Series, which includes the following report types:

- TECHNICAL PUBLICATION. Reports of completed research or a major significant phase of research that present the results of NASA programs and include extensive data or theoretical analysis. Includes compilations of significant scientific and technical data and information deemed to be of continuing reference value. NASA counter-part of peer-reviewed formal professional papers, but has less stringent limitations on manuscript length and extent of graphic presentations.
- TECHNICAL MEMORANDUM. Scientific and technical findings that are preliminary or of specialized interest, e.g., “quick-release” reports, working papers, and bibliographies that contain minimal annotation. Does not contain extensive analysis.
- CONTRACTOR REPORT. Scientific and technical findings by NASA-sponsored contractors and grantees.
- CONFERENCE PUBLICATION. Collected papers from scientific and technical conferences, symposia, seminars, or other meetings sponsored or co-sponsored by NASA.
- SPECIAL PUBLICATION. Scientific, technical, or historical information from NASA programs, projects, and missions, often concerned with subjects having substantial public interest.
- TECHNICAL TRANSLATION. English-language translations of foreign scientific and technical material pertinent to NASA's mission.

For more information about the NASA STI program, see the following:

- Access the NASA STI program home page at <http://www.sti.nasa.gov>
- E-mail your question to help@sti.nasa.gov
- Fax your question to the NASA STI Information Desk at 757-864-6500
- Telephone the NASA STI Information Desk at 757-864-9658
- Write to:
NASA STI Program
Mail Stop 148
NASA Langley Research Center
Hampton, VA 23681-2199



Supersonic Inlet Test for a Quiet Supersonic Transport Technology Demonstrator in the NASA Glenn 8- by 6-Foot Supersonic Wind Tunnel

*Raymond Castner and Stephanie Simerly
Glenn Research Center, Cleveland, Ohio*

*Michael Rankin
Lockheed Martin, Palmdale, California*

Prepared for the
Applied Aerodynamics Conference
sponsored by the American Institute of Aeronautics and Astronautics
Atlanta, Georgia, June 25–29, 2018

National Aeronautics and
Space Administration

Glenn Research Center
Cleveland, Ohio 44135

Acknowledgments

This work was funded by the NASA Commercial Supersonics Technology Project. The demonstrator vehicle wind tunnel model was designed, fabricated and tested under a contract with the Lockheed Martin Corporation. Appreciation is extended to the staff at the NASA Glenn Research Center 8- by 6-foot Supersonic Wind Tunnel in Cleveland, Ohio; this test would not have been possible without their dedication and countless hours of hard work to make this test a success.

This work was sponsored by the Integrated Aviation Systems Program at the NASA Glenn Research Center.

Level of Review: This material has been technically reviewed by technical management.

Available from

NASA STI Program
Mail Stop 148
NASA Langley Research Center
Hampton, VA 23681-2199

National Technical Information Service
5285 Port Royal Road
Springfield, VA 22161
703-605-6000

This report is available in electronic form at <http://www.sti.nasa.gov/> and <http://ntrs.nasa.gov/>

Supersonic Inlet Test for a Quiet Supersonic Transport Technology Demonstrator in the NASA Glenn 8- by 6-Foot Supersonic Wind Tunnel

Raymond Castner and Stephanie Simerly
National Aeronautics and Space Administration
Glenn Research Center
Cleveland, Ohio 44135

Michael Rankin
Lockheed Martin
Palmdale, California 93599

Abstract

NASA funded the preliminary design of a flight demonstrator aircraft with a greatly reduced sonic boom signature to enable supersonic flight over land. In 2017, two tests were performed at the NASA Glenn Research Center 8- by 6-foot Supersonic Wind Tunnel, an aerodynamic stability/control test and an inlet performance test. The inlet was unique due to the location on the vehicle, located on the top centerline near the rear of the aircraft. Test data provided a validation and performance dataset for engine integration on the demonstrator vehicle. The subject of this report is the subsonic and supersonic performance data collected for the centerline top-mounted inlet.

Nomenclature

8x6	SWT 8- by 6-foot Supersonic Wind Tunnel
AIP	aerodynamic interface plane
GRC	NASA Glenn Research Center
IDCMAX	maximum value circumferential inlet distortion
IDRMAX	maximum value radial inlet distortion
LBFD	Low Boom Flight Demonstrator
m_2	inlet airflow, station 2, lbm/sec
M_∞	free-stream Mach number
m_o	inlet capture flow, lbm/sec
P_{t2}	average AIP total pressure, station 2, psia
P_{tbl}	boundary layer rake total pressure, psia
$P_{t\infty}$	freestream total pressure, psia
QueSST	Quiet Super Sonic Transport
VG	vortex generator
α	angle of attack or pitch, degrees
β	angle of sideslip or yaw, degrees

1.0 Introduction

NASA is developing technology to reduce the annoyance of supersonic overland flight and to enable public supersonic air travel. An important step in this research was to develop a Quiet Super Sonic

Transport (QueSST) preliminary design. The preliminary design was for a technology demonstrator experimental aircraft (x-plane) that will be flown by the Low Boom Flight Demonstrator (LBFD) Project. At approximately 100 ft in length, the LBFD design was smaller than a future supersonic aircraft, but designed to replicate its sonic boom signature. With a cruise Mach number of Mach 1.43 the low-boom design was developed through computer analysis and shape optimization. One key feature was the use of the airframe to shield the propulsion system and minimize its effect on sonic boom. This top centerline inlet location created challenges with ingestion of fuselage boundary layer flow, which could reduce engine performance. The vehicle utilized a diverter-less bump inlet to address the performance challenges of the unique top centerline location.

As part of the demonstrator vehicle design, two wind tunnel tests were performed at the NASA Glenn Research Center (GRC). The first test was an aerodynamic stability and control test. Second was a propulsion test to study static, low speed, and high speed inlet performance of the top-mounted inlet. These tests were combined into one test entry in 2017 and took place at the GRC 8- by 6-foot Supersonic Wind Tunnel (8x6 SWT) in Cleveland, Ohio.

Two different inlet configurations were tested: (1) a C607.2 inlet (called the C607 inlet for the remainder of this report) was the basis for the installed propulsion database leading into the LBFD program's preliminary design review and (2) modifications to this inlet, resulting in the C608.1 inlet (called C608). The C608 inlet had a 3.5 percent larger throat area (528 in.² versus C607 510 in.² full scale). The bump was also recontoured in the C608 to increase the shock strength and increase removal of the boundary layer. The C608 internal lip radius was doubled from the C607 design to improve take-off and crosswind engine operability.

Propulsion-airframe integration effects on the inlet were not known for top-mounted inlets; as a result the entire vehicle was included for the propulsion test. The effects on inlet performance of the vehicle nose, canards, cockpit, forward camera pod, and top-mounted vortex generators were assessed. A 9.5 percent scale model was selected, which was the largest full vehicle wind tunnel model tested to date in the 8x6 SWT test section. The inlet was 3-in. diameter at the engine aerodynamic interface plane (AIP) and the Reynolds number was 4 times lower than the flight conditions for the full scale vehicle. This difference in Reynolds number produced results in agreement with full scale vehicle analysis, and is consistent with conclusions made by Norby (Ref. 1).

The forward vision camera pod and the vortex generators can influence boundary layer growth and inlet performance. Initial computational analysis gave conflicting results depending on the code used and the assumptions applied. The camera-on versus camera-off cases were used to determine the effect of a forebody camera on inlet performance. A boundary layer rake was also added to the top centerline of the model in front of the inlet to quantify the effects of the camera or the vortex generators. Final results demonstrated that only the vortex generators had an effect on the inlet performance. The two configurations with and without the camera fairing had no effect on the C607 inlet performance. Camera fairing data are not presented.

The subject of this report is the subsonic and supersonic inlet performance data collected for the centerline top-mounted, aft-mounted, diverter-less bump inlet geometries. The purpose is to document the inlet pressure recovery and distortion from static conditions to cruise conditions. Effects of vortex generators and inlet performance variation with vehicle pitch and yaw will be presented.

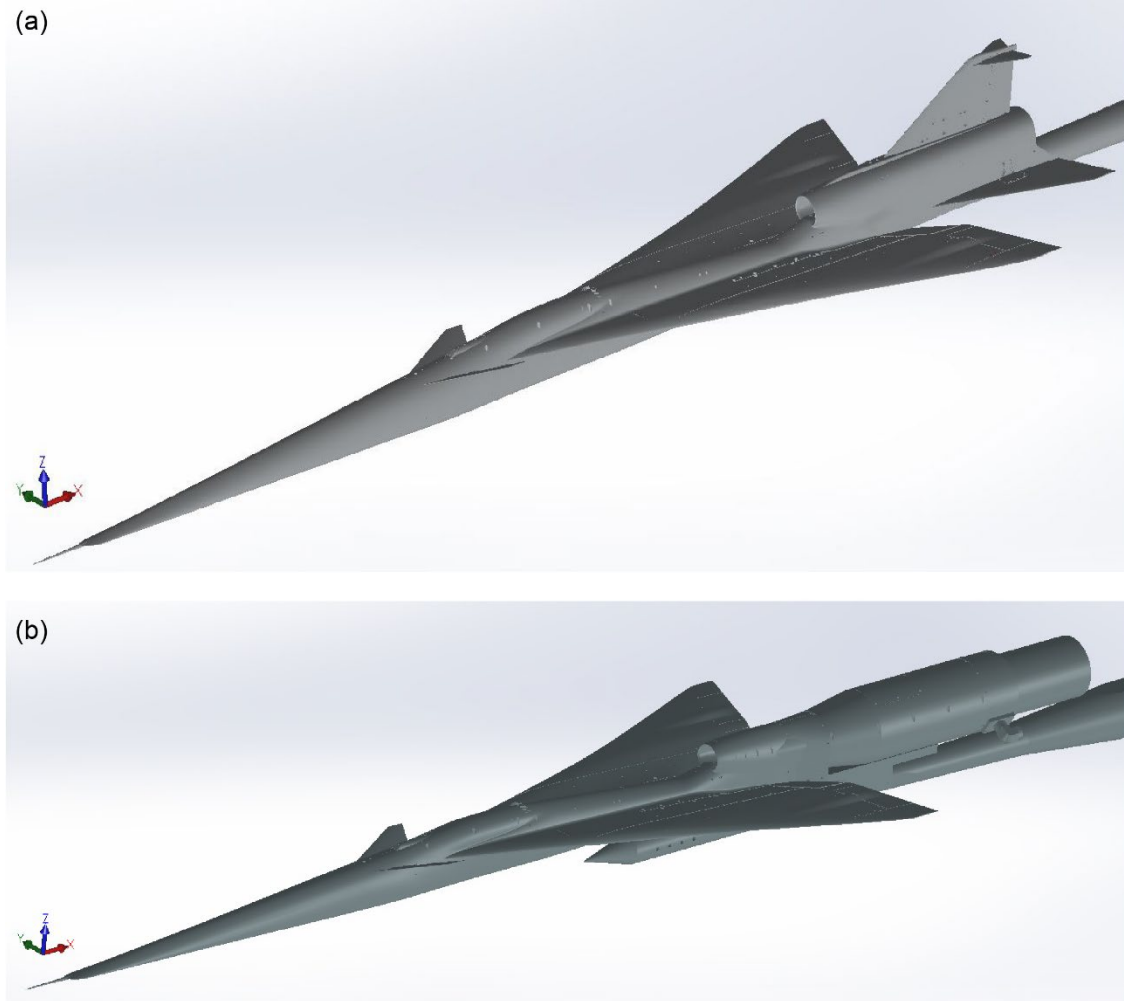


Figure 1.—(a) Aerodynamic configuration, and (b) propulsion configuration.

2.0 Experimental Setup

2.1 Test Setup

A common wind tunnel model assembly was modified for both the aerodynamic stability and control test and the propulsion test. The common model assembly is shown in Figure 1, with both the aerodynamic configuration and the propulsion configuration. The model was 106.54 in. from the tip of the nose to the horizontal stabilizer trailing edge tip (Figure 2). For the propulsion test, the common model was removed from the sting and mounted on a small blade-strut, to accommodate the propulsion mass-flow plug assembly, see Figure 3 and Figure 4.

A set of vortex generators were present on the vehicle fuselage aft of the cockpit. To better understand how the configurations influenced the boundary layer to reduce inlet distortion, four different vortex generator configurations were tested: 1) None, 2) C607 baseline, 3) C607 alternate, and 4) C608 baseline (Figure 5). Configurations had differences in height, chord, spacing, number, and deflection; dimensions are outlined in Table I. All configurations were flat plates arranged to generate co-rotating vortex patterns on the top of the fuselage with vortex rotations counter-clockwise looking downstream on the port side and clockwise looking downstream on the starboard side. The forward camera fairing was a fixed geometry that could be removed, resulting in the two possible configurations of camera-on and camera-off.

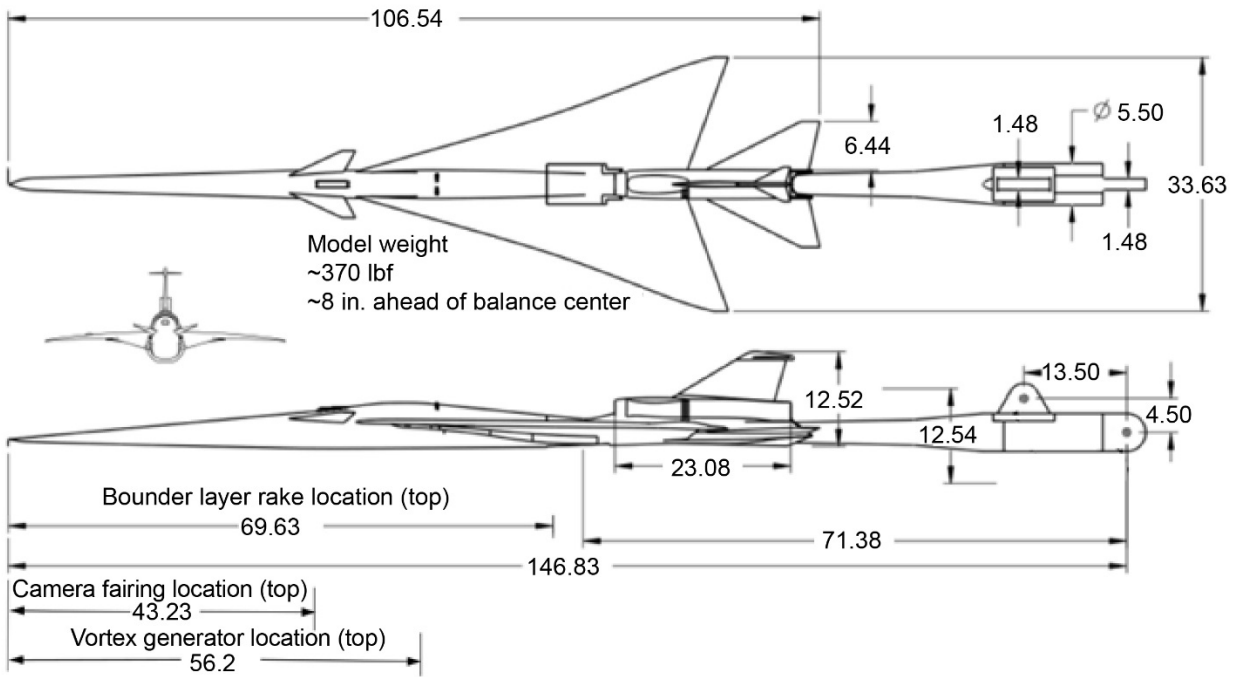


Figure 2.—Dimensions (in inches??).

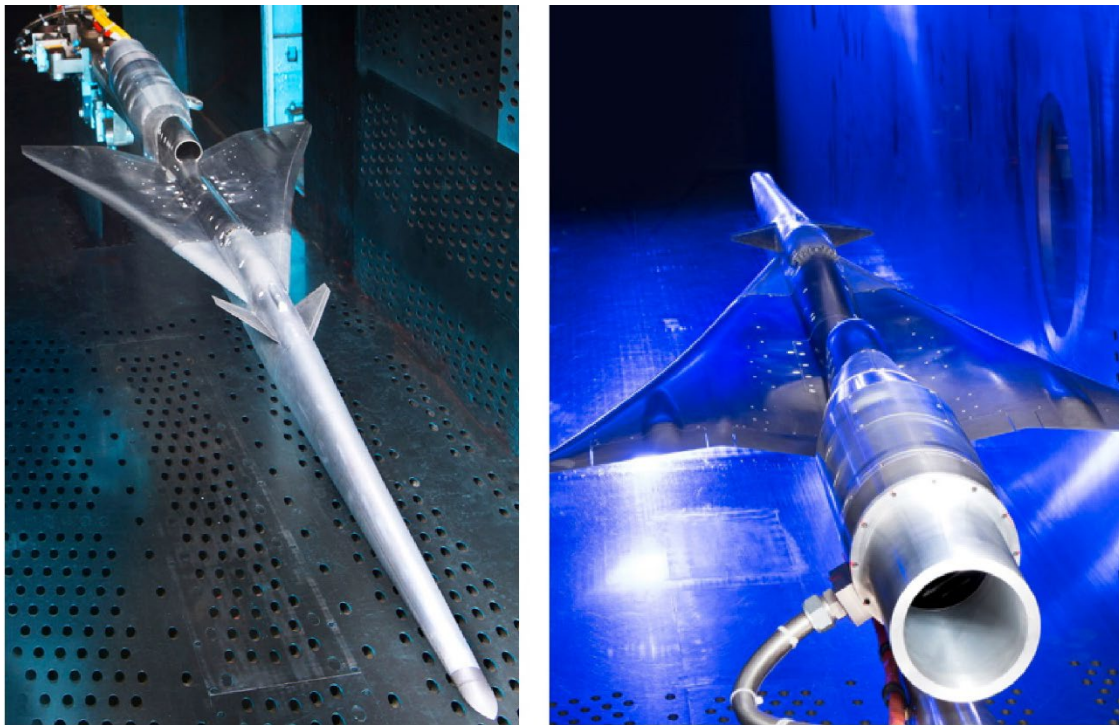


Figure 3.—Propulsion model in 8x6 SWT.

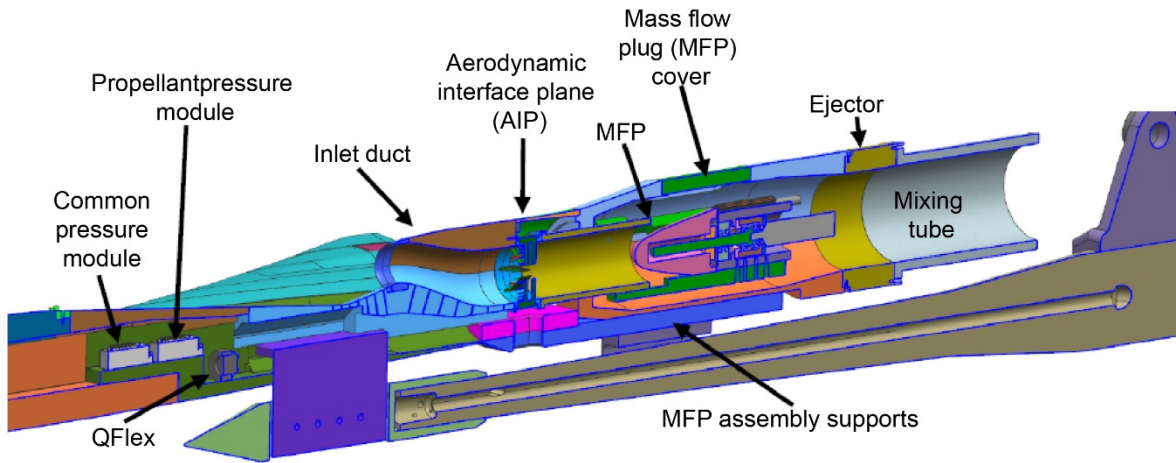


Figure 4.—Propulsion model.



Figure 5.—Vortex generator configurations (see Table I for dimensions). (a) No VG. (b) C607 Baseline. (c) C607 Alternate. (d) C608 Baseline.

TABLE I.—VORTEX GENERATOR (VG) DIMENSIONS, MODEL SCALE

VG	Height, in.	Chord, in.	Spacing, in.	Deflection, deg	Number
None	-----	-----	-----	--	--
C607 Baseline	0.263	0.421	0.368	15	8
C607 Alternate	0.053	0.263	0.210	20	16
C608 Baseline	0.105	0.526	0.421	20	8

The 8x6 SWT transonic test section was configured with 5.8 percent porosity (Ref. 2). To fit in the transonic test section, the model was sting-mounted on the transonic strut. This strut had lower load capabilities than the 8x6 SWT supersonic strut located forward in the test section. Therefore, to protect the transonic strut, angle of attack was limited at supersonic speeds from -2° to 5° ; at transonic speeds from -2° to 8° ; and at subsonic speeds from -4° to 14° .

2.2 Instrumentation

Instrumentation included static pressure measurements on the vehicle surface, total pressure measurements at the AIP where the engine fan would be located, and instrumentation both upstream and downstream of the mass flow plug (4 total pressure probes ahead of the plug plus 8 aft facing static pressure measurement locations). AIP fan face measurements were collected with an array of 40 total pressure probes (Figure 6) where the probe locations were defined per the SAE standard (Ref. 3). Locations for the total pressure probes at the 3-in. diameter AIP are detailed in Table II. No simulated engine center body was included. Four high-response dynamic pressure probes were also included at the AIP, but are not the focus of this report. The dynamic measurements were used to check for inlet buzz, which did not occur during most testing except at very low airflow and high angles of sideslip. For a limited number of test conditions at the end of the test a boundary layer rake was installed. The rake was located at a fuselage station of $x = 69.625$ in. from the tip of the nose, with probe locations as shown in Table II.

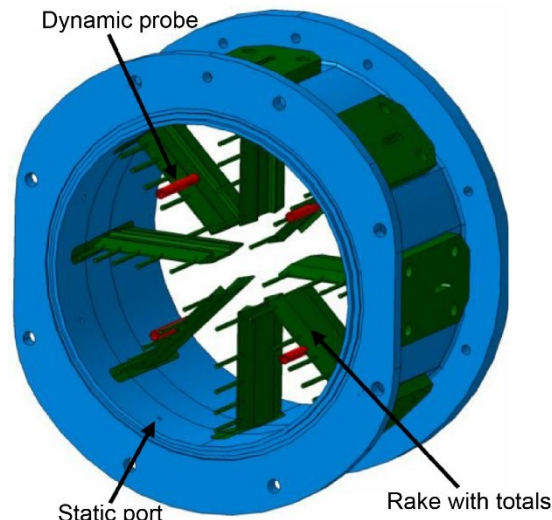


Figure 6.—Aerodynamic Interface Plane (AIP) instrumentation.

TABLE II.—AERODYNAMIC INTERFACE PLANE AND BOUNDARY LAYER RAKE INSTRUMENTATION LOCATIONS

Aerodynamic Interface Plane (AIP)				Boundary layer rake	
Probe ID	Radial location, in.	Rake ID	Angular location	Probe ID	Height above surface, in.
1	0.466	1	0	1	0.05
2	0.807	2	45	2	0.15
3	1.041	3	90	3	0.10
4	1.232	4	135	4	0.30
5	1.397	5	180	5	0.50
-	-----	6	225	6	0.75
-	-----	7	270	-	1.05

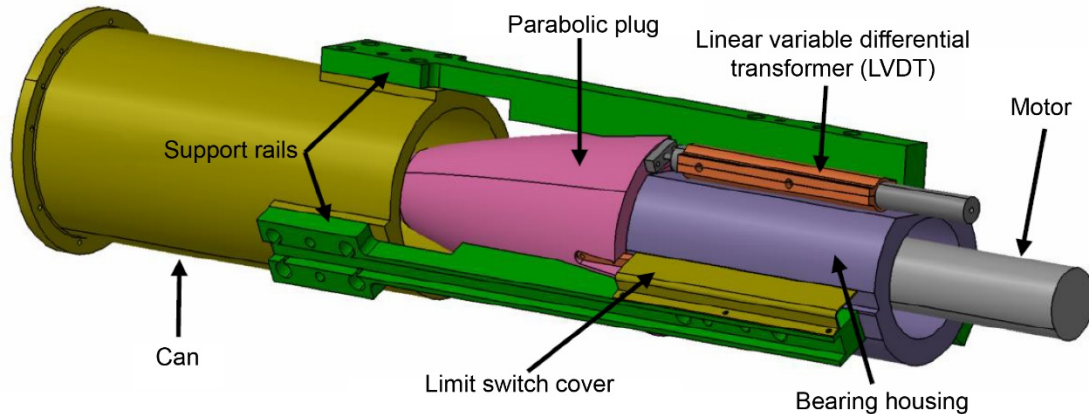


Figure 7.—Mass flow plug.

2.3 Mass Flow Plug (MFP)

A calibrated mass flow plug was mounted aft of the subsonic diffuser and was used to control airflow through the inlet. The 3-in. diameter assembly included a parabolic plug to maintain a linear mass flow versus position characteristic as the plug position was varied during operation. The plug was mounted on a linear ball-screw assembly with 2.5 in. of travel (Figure 7). For both supersonic and high-subsonic operation the mass flow plug was choked. Upstream and downstream pressure measurements were used to verify choked flow operation. For low-subsonic operation, an air-driven ejector was installed behind the mass flow plug to maintain choked flow; the ejector was present during the entire test but only operated when needed. At low subsonic Mach numbers the mass flow plug was operated unchoked, as the ejector was not able to maintain low pressure at the plug exit. A post-test calibration was performed to characterize unchoked operation.

2.4 Measurement Uncertainty and Test Procedure

AIP pressure measurements were measured with ± 15 psi pressure modules with measurement uncertainty of ± 0.015 psi. When combined with measurement uncertainties in the 8x6 SWT wind tunnel (Ref. 4), overall measurement uncertainty for total pressure recovery was estimated at ± 0.00375 . To account for the pneumatic lag in the pressure measurement tubing, standard deviations of recovery measurements were monitored. Data was collected after 5 to 10 sec of dwell time at a test condition, when the standard deviations reached steady-state values.

Uncertainty for the wind tunnel Mach number was within ± 0.0054 , for flow angularity was $\pm 0.5^\circ$, and for wind tunnel total temperature was ± 2.4 R (Ref. 5). Accuracy of model pitch and roll were 0.05° and 0.06° .

The mass flow plug was calibrated before and after the test. For clean inflow the mass flow uncertainty was estimated to be ± 0.5 percent. With highly distorted inflow the mass flow uncertainty was less than ± 2 percent. At each test condition the mass flow plug was actuated to determine the inlet performance as a function of inlet back pressure. Approximately 8 to 10 data points were collected for each mass flow plug sweep, with points concentrated around the critical point. The inlet critical point was identified as the point of maximum total pressure recovery at the maximum mass capture (just before subcritical spillage at the cowl lip).

3.0 Experimental Results

Results are summarized for both supersonic and subsonic Mach numbers. All data are presented with the post-test mass flow plug calibration. Steady-state inlet recovery was measured with the 40-probe array located at the AIP. Measurements from the 40 probes were averaged and normalized to freestream pressure. Inlet distortion is also presented, where the General Electric values of IDC and IDR are used (Ref. 6). These values are similar to the SAE ARP 1420 standard (Ref. 3), where IDR equals DPRP and IDC is similar to DPCP with a modified extent factor. Maximum values for each were used for the determination of IDC_{MAX} and IDR_{MAX}.

3.1 C607 Supersonic Inlet Performance

Figure 8 shows C607 inlet performance with the C607 baseline vortex generators installed on the aircraft. The mass flow ratio was computed based on the inlet throat area (4.603 in.²) and did not include the precompression surface of the centerline top-mounted inlet bump diverter. The actual Mach number at the inlet aperture was not measured and the capture area including the precompression area was not estimated. As a result, mass flow ratio values greater than 1.0 are reported. Recovery for supersonic Mach numbers between 1.08 and 1.55 are shown with respect to the inlet mass flow ratio, m_2/m_0 (Figure 8(a)). The critical point was determined for each Mach number and these critical point values were used to assess the effect of vehicle attitude on inlet performance. Note that the critical point is not the point of highest recovery for this diverter-less bump inlet. The inlet can be operated in the subcritical portion of the performance curve, where a tradeoff is made between increased inlet recovery and increased spillage drag.

Figure 8(b) shows the effect of vehicle attitude and Mach number on the inlet mass flow at critical points. As expected, there was an increase in mass flow ratio as flight Mach number increased and the shock wave structure from the bump became steeper. Mass capture values increased from 0.94 to 1.1 as Mach number was increased from 1.08 to 1.55 and were not sensitive to changes in vehicle attitude. The effect of vehicle attitude and Mach number on inlet recovery is shown in Figure 8(c). Recovery decreased from 0.98 to 0.905 as Mach number was increased from 1.08 to 1.55. Recovery was also insensitive to changes in vehicle attitude, except for the flight condition at $\alpha = -2^\circ$ and $\beta = -2^\circ$ which reduced recovery to 0.90 at Mach 1.45. Inlet distortion was also assessed at the critical point. Effects on distortion are presented for the same vehicle attitudes and Mach numbers as shown in Figure 8(b) and Figure 8(c). Steady-state values of IDC_{MAX} were at or below 0.1 (Figure 8(d)) with the exception of results at $\beta = -2^\circ$ where values were reported as high as 0.15. Values for IDR_{MAX} were largely at or below 0.06. Use of these steady-state distortion values, compared to engine operability limits, can be made on a case-by-case basis depending upon the engine selected. Mach number contours at the vehicle aerodynamic interface plane (AIP) are presented in Figure 9. Data is presented for the critical point at the tested vehicle attitudes. With the C607 baseline vortex generators, changes in angle of attack and sideslip did not have a dramatic effect on the Mach contours. Only at values of $\alpha = -2^\circ$ and $\beta = -2^\circ$ was there a noticeable difference, where the increased level of flow distortion can be clearly seen in the Mach contour plot. This trend was the same at all vehicle Mach numbers and plots for additional Mach numbers are not shown in this report.

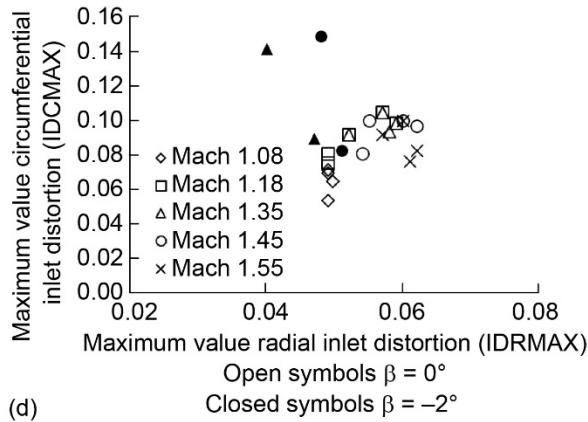
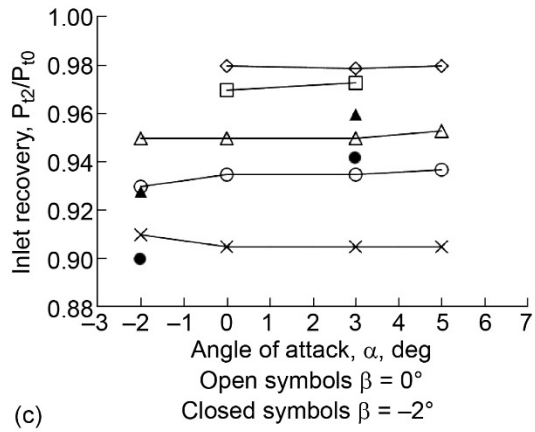
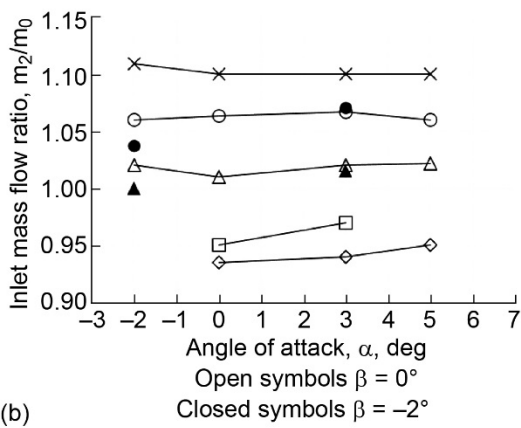
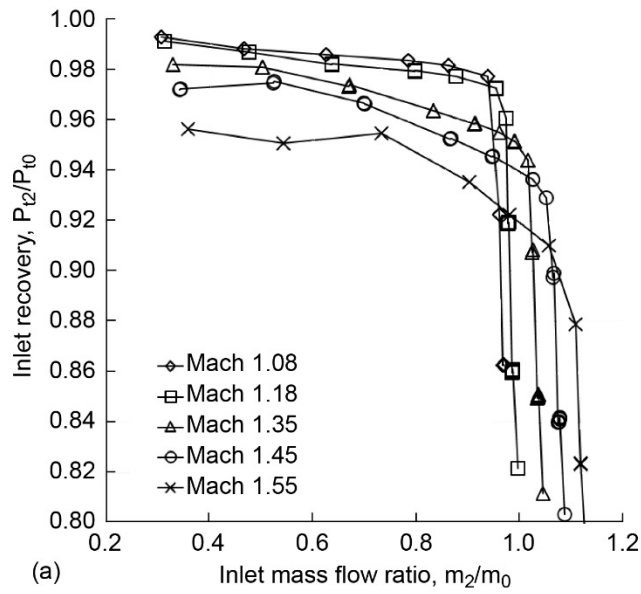


Figure 8.—(a) C607 Supersonic inlet performance, $a = 0^\circ$, $b = 0^\circ$, baseline vortex generator set, (b) Supersonic inlet mass flow ratio at the critical point, (c) Supersonic inlet recovery at the critical point, and (d) Inlet distortion at the critical point.

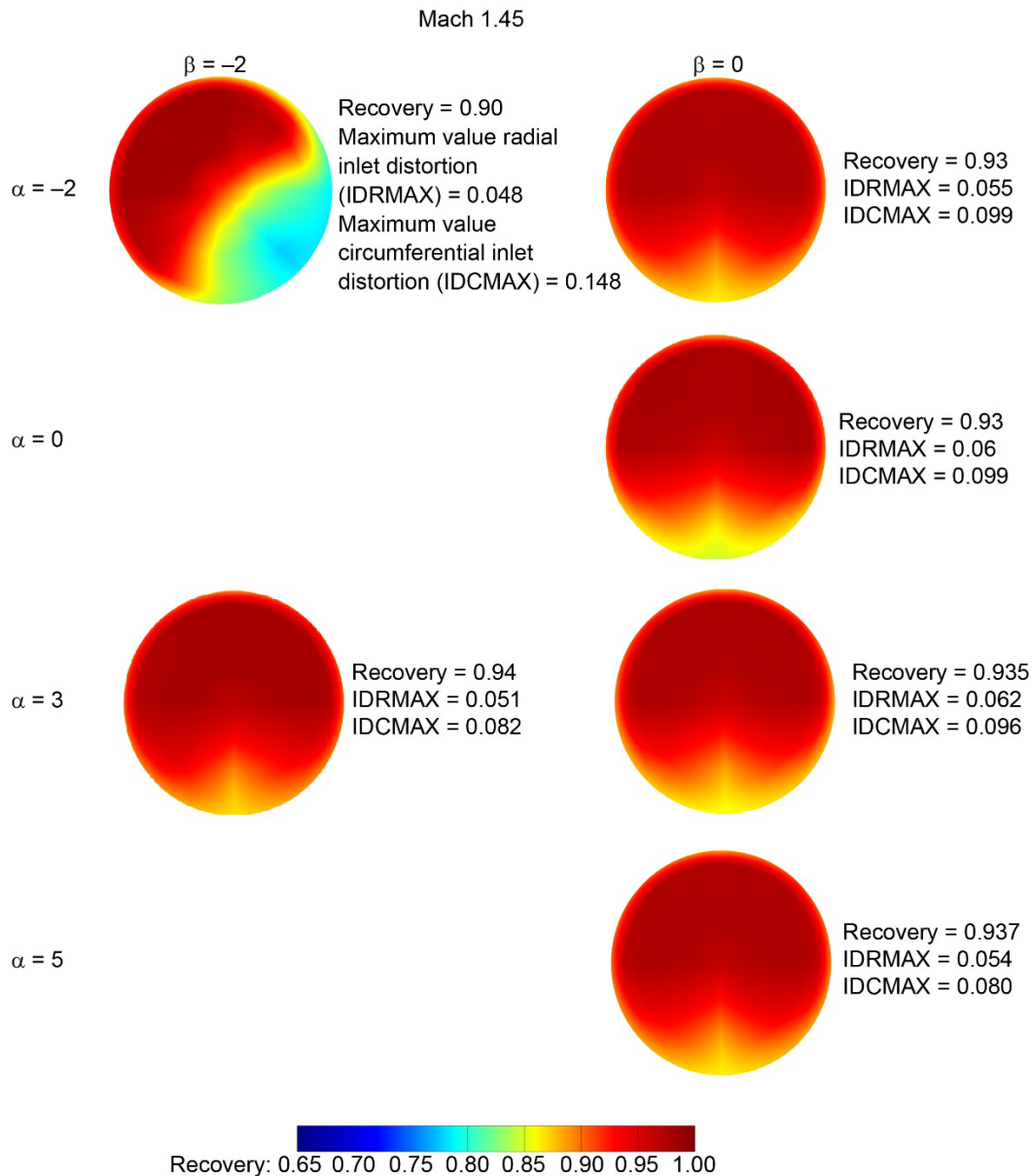


Figure 9.—C607 Mach 1.45 AIP pressure recovery contour plots at the critical point, baseline vortex generator set.

The C607 inlet was tested with two sets of vortex generators, where the baseline set was longer (0.263 in.) than the alternate set (0.053 in.). A configuration was also tested with vortex generators removed. Vortex generators were tested near the vehicle cruise condition at Mach 1.45. The effects of the vortex generators are shown in Figure 10(a) and (b) where the longer baseline vortex generators exhibited highest levels of inlet performance. The effect of the vortex generator type was dramatic, resulting in 5 percent improvement in inlet recovery over the case with no vortex generators at $\alpha = 3^\circ$, and a corresponding but smaller improvement in mass flow ratio. At $\alpha = 0^\circ$ the baseline vortex generators had an 8 percent improvement in inlet recovery over the case with no vortex generators. The C607 alternate vortex generator configuration demonstrated reduced performance over the C607 baseline generators, and had increased sensitivity to vehicle attitude with sideslip. The baseline vortex generators demonstrated the lowest levels of distortion (Figure 10(c)). Values of IDRMAX were below 0.06 and IDCMAX were

below 0.12. The impact of the vortex generator type on the AIP Mach number contour plots is shown in Figure 10(d). Results indicate the importance of having effective vortex generators mounted on the fuselage upstream of this centerline top-mounted inlet.

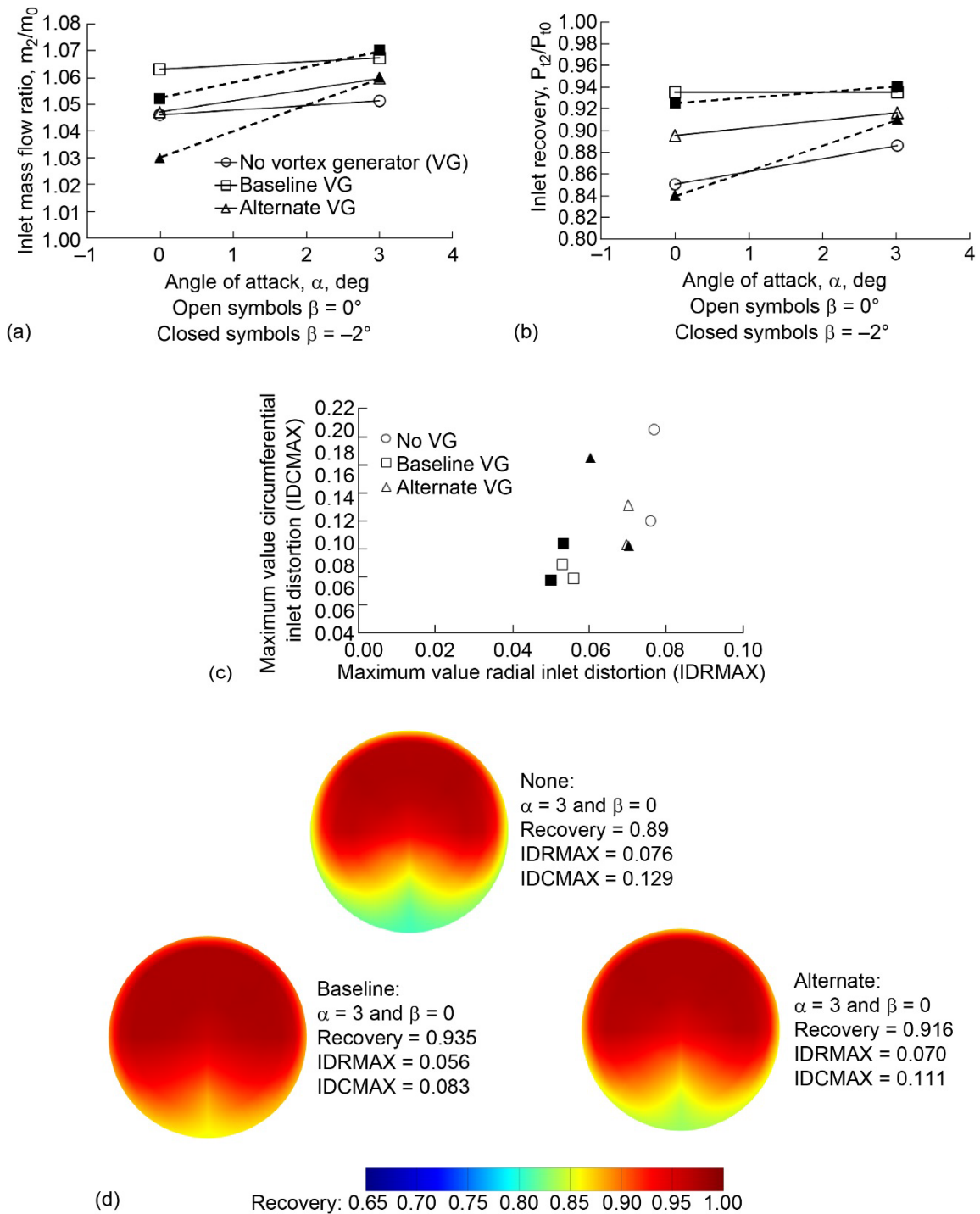


Figure 10.—C607 Mach 1.45 vortex generator comparisons (a) Effect of α and β on mass flow ratio, (b) Effect of α and β on critical point inlet recovery, (c) Critical point inlet distortion, and (d) AIP pressure recovery contour plots at the critical point.

The C607 inlet was also tested with a total pressure measurement rake located on the centerline in front of the inlet to characterize the incoming inlet boundary layer flow profile. The motivation for these measurements was to make comparison to computational fluid dynamics computations near the cruise angle of attack ($\alpha = 2^\circ$). Comparison of Figure 11(a) and (b) demonstrate that a thicker boundary layer evolved from the shorter alternate vortex generator configuration. This thicker boundary layer had a negative impact on inlet recovery as previously presented in Figure 10. There was no change in boundary layer profiles with vehicle angle of attack (Figure 11(c) and (d)).

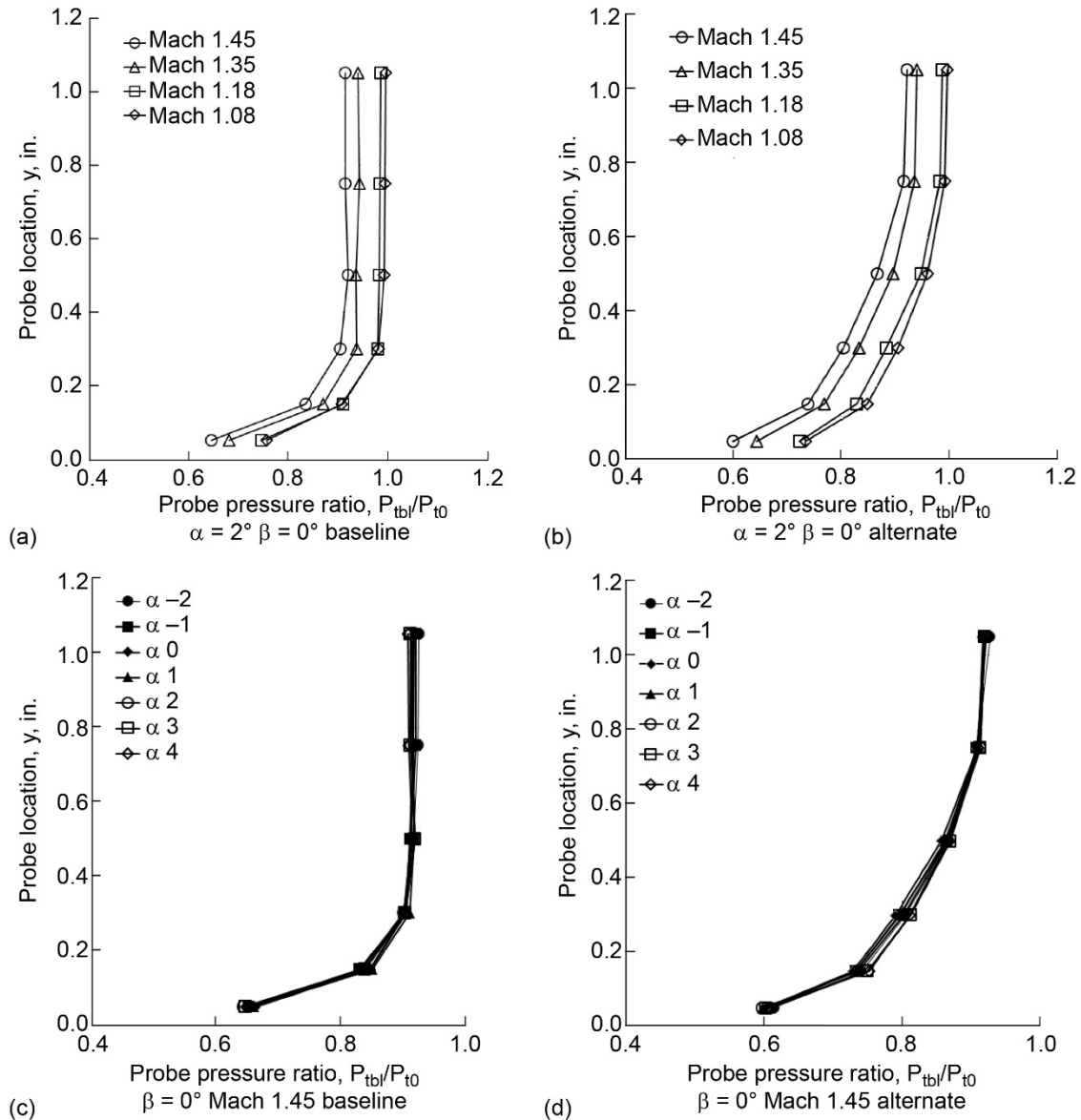


Figure 11.—C607 Boundary layer rake measurement, $a = 2^\circ$, $b = 0^\circ$, (a) Baseline vortex generator set variation with Mach number, (b) Alternate vortex generator set variation with Mach number, (c) Baseline vortex generator set variation with angle of attack, and (d) Alternate vortex generator set variation with angle of attack.

3.2 C608 Supersonic Inlet Performance

C608 inlet performance is presented with the C608 baseline vortex generators installed on the aircraft. Inlet recovery for supersonic Mach numbers between 1.08 and 1.55 is shown with respect to the inlet mass flow ratio (Figure 12(a)). The mass flow ratio was computed based on the inlet throat area (4.765 in.² versus 4.603 in.² for the C607) in the same way as done for the C607 inlet. Mass flow ratio values greater than 1.0 are again reported. Figure 12(b) shows the effect of vehicle attitude and Mach number on the inlet mass flow at these identified critical points. Trends show an increase in mass flow ratio from 0.97 to 1.1 as Mach number was increased from 1.08 to 1.55. The trends in mass flow ratio were similar to the C607 inlet and were not sensitive to vehicle attitude. When compared to the C607 inlet, the mass flow capture for the C608 inlet increased by 0.02. The increase in mass capture was likely due to differences in geometry of the bump diverter between the C607 and C608 inlets. The recovery (Figure 12(c)) was also not sensitive to changes in vehicle attitude. Inlet recovery decreased from 0.98 to 0.91 as Mach number was increased from 1.08 to 1.55. Recovery for the C608 inlet was comparable to the C607 inlet at the critical point. Changes in sideslip caused a large reduction in recovery, to 0.88 at Mach 1.45. Inlet distortion was again assessed at the critical point. Effects on distortion are presented for the same vehicle attitudes and Mach numbers as shown in Figure 12(b) and (c). Values of IDC_{MAX} were at or below 0.1 (Figure 12(d)) with exception of results at $\beta = -2^\circ$ where values were reported as high as 0.16. Values for IDR_{MAX} were below 0.08. At the critical point, maximum values for both IDR_{MAX} and IDC_{MAX} were slightly greater than the 3 percent smaller C607 inlet.

3.3 C607 Subsonic Inlet Performance

Subsonic performance data was collected for the C607 inlet between Mach 0 and Mach 0.9 (Figure 13(a)). As an example, the trends in recovery are presented at a mass flow per unit area of 0.26, or 132 lbm/sec corrected flow for the full scale vehicle. Recovery was reduced from 0.992 to 0.98 as Mach number was increased from Mach 0.25 to Mach 0.9 (Figure 13(b)). Performance for these Mach numbers was not significantly affected by changes in vehicle angle of attack. Recovery at both Mach 0.6 and 0.8 was reduced by 0.5 percent at $\beta = -2^\circ$. Static inlet performance was significantly lower than the performance at all other Mach numbers, with recovery of 0.89 at a mass flow per unit area of 0.26. This behavior is typical for a supersonic inlet with thin-lip losses. Inlet distortion values are shown in Figure 13(c) for the same mass flow per unit area and the same vehicle attitudes as Figure 13(b). Distortion values were not sensitive to the vehicle attitude. For this mass flow, the distortion values for IDR_{MAX} were below 0.03. One exception was at the Mach 0.9 flight condition where IDR_{MAX} was 0.0375. The IDC_{MAX} distortion values were below 0.06. One exception was at the Mach 0 flight condition where IDC_{MAX} was 0.1

3.4 C608 Subsonic Inlet Performance

Performance data was also collected for the C608 inlet (Figure 14(a)) between Mach 0 and Mach 0.9. Again as an example the trends in recovery are presented at a mass flow per unit area of 0.26, or 137 lbm/sec corrected flow for the full scale vehicle. The C608 inlet performance trends were similar to the C607 inlet. At Mach 0.8 and Mach 0.9 the inlet recovery was 0.5 percent higher than the C607. Recovery was reduced from 0.992 to 0.985 as Mach number was increased from Mach 0.25 to Mach 0.9 (Figure 14(b)). Performance for these Mach numbers was not affected by changes in vehicle angle of

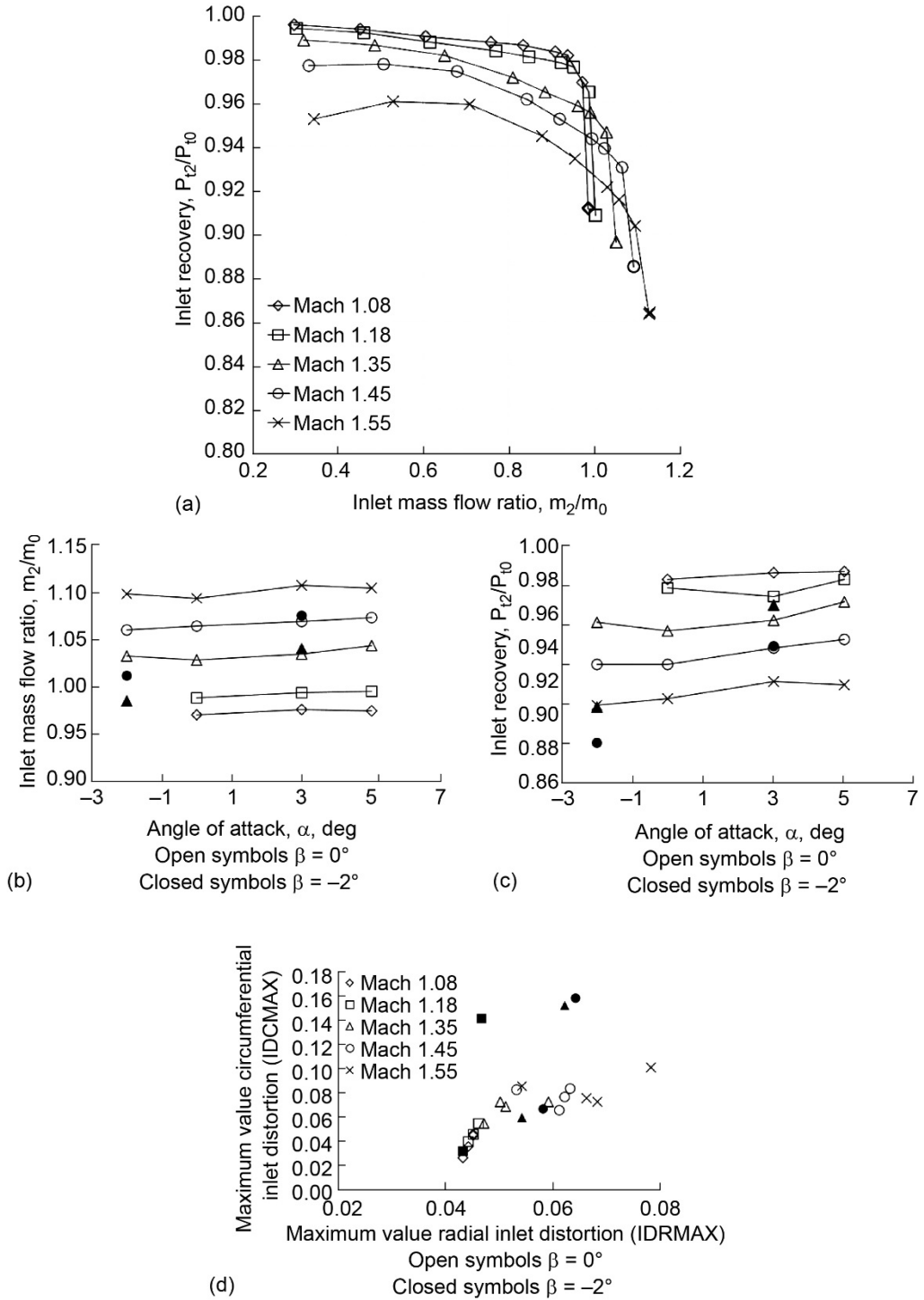


Figure 12.—(a) C608 inlet recovery, $\alpha = 3^\circ$, $\beta = 0^\circ$, C608 vortex generator set, (b) Critical point inlet mass flow ratio, (c) Critical point inlet recovery, and (d) Inlet distortion at the critical point.

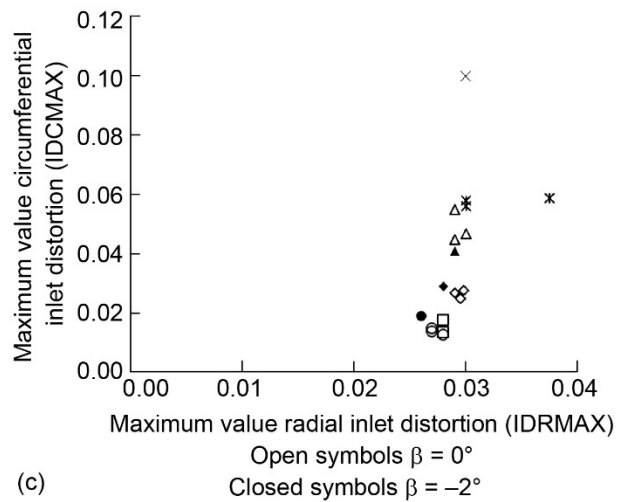
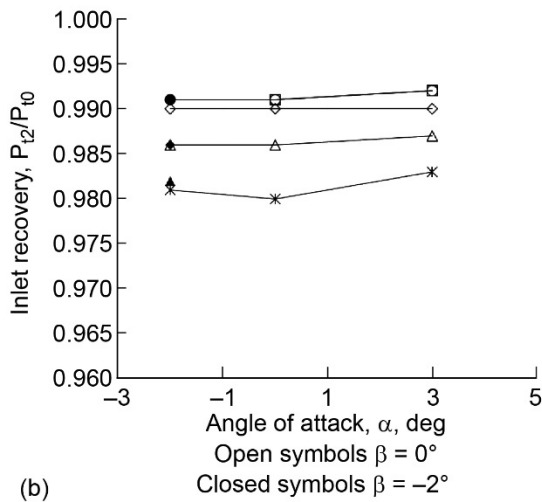
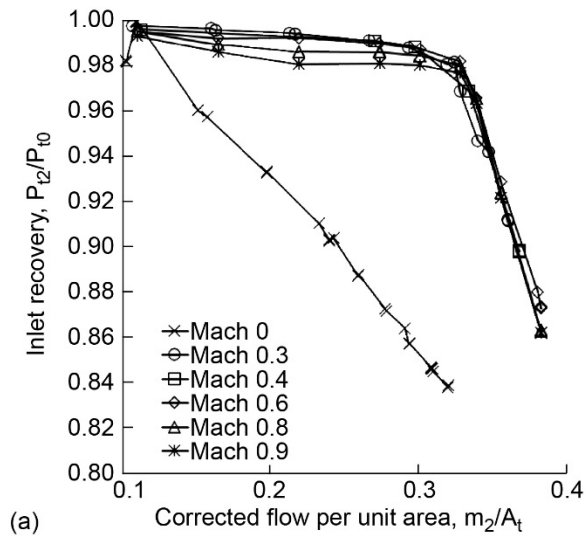


Figure 13.—C607 (a) Subsonic inlet performance $a = 0^\circ$, $b = 0^\circ$, (b) Inlet performance variation with vehicle attitude, and (c) IDC Maxwell vs. IDR Maxwell variation with vehicle attitude.

attack. Recovery at Mach 0.8 was reduced by 1.75 percent at $\beta = -2^\circ$. Static performance was again significantly lower than the performance for all other Mach numbers. With the increased lip radius and increased area, the C608 inlet performance was expected to have a lower throat Mach number, reduced lip losses, and higher recovery. When compared to C607, static performance increased to 0.90, or 1 percent over the C607 at a mass flow per unit area of 0.26. Inlet distortion values are shown in Figure 14(c) for the same mass flow per unit area and the same vehicle attitudes as Figure 14(b). Distortion values for the C608 again were not sensitive to the vehicle attitude, with exception that the C608 inlet had a higher sensitivity to flight conditions at $\beta = -2^\circ$. At zero sideslip angles, IDR Maxwell was below 0.025 and IDC Maxwell was below 0.04. With increased sideslip angle, $\beta = -2^\circ$, IDC Maxwell increased to 0.06. The maximum value for IDC Maxwell was for the static flight condition.

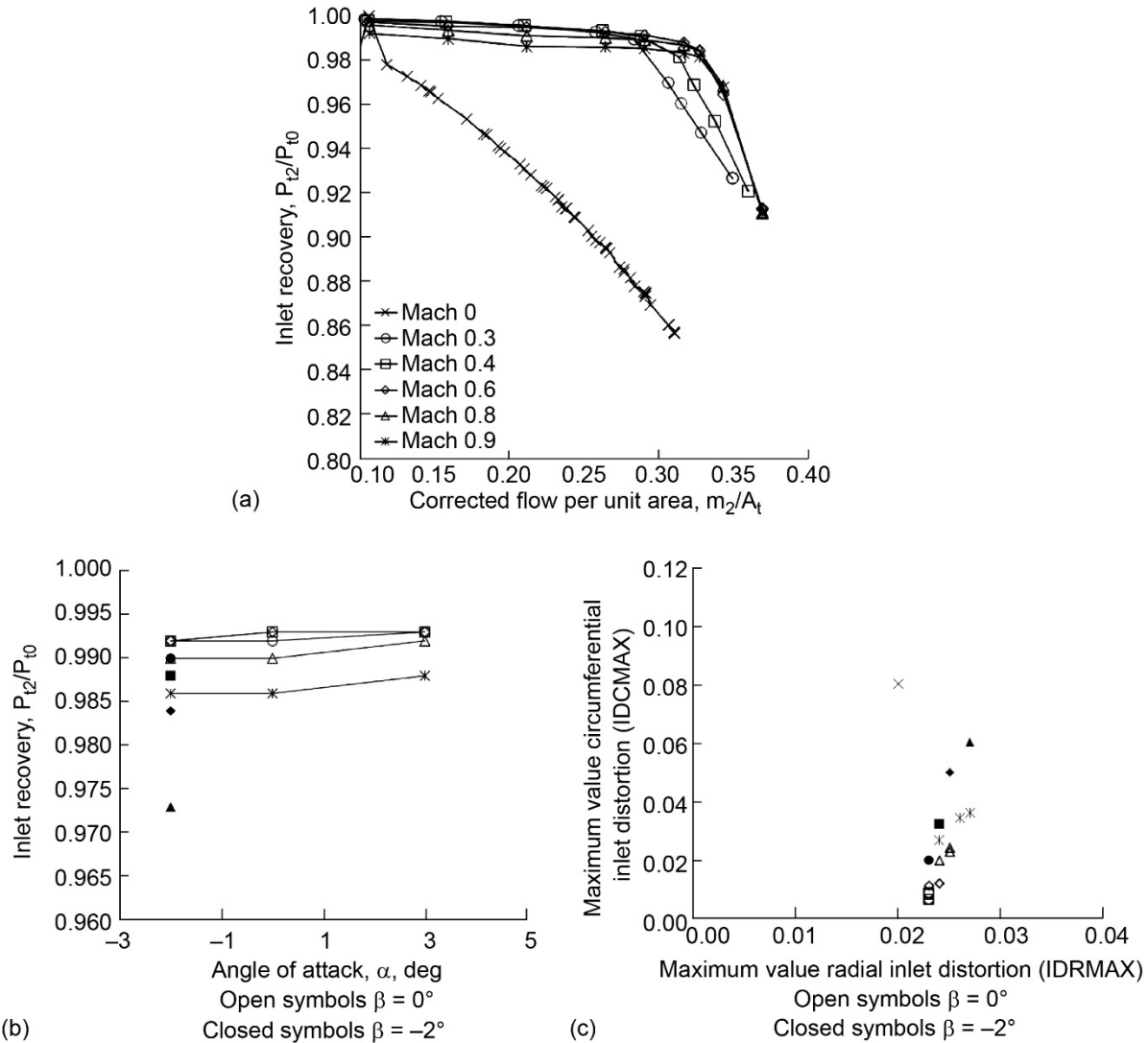


Figure 14.—C608 (a) Subsonic inlet performance $a = 0^\circ$, $b = 0^\circ$, (b) Inlet performance variation with vehicle attitude, and (c) IDC MAX vs. IDR MAX variation with vehicle attitude.

4.0 Summary and Conclusions

As part of the Lbfd demonstrator vehicle preliminary design, two wind tunnel tests were performed. The first test was an aerodynamic stability and control test, and the second was a propulsion test to study both low speed and high speed inlet performance. These tests were combined into one test entry in 2017 and took place at the 8x6 SWT. Inlet performance data were collected for two inlet designs, including inlet recovery and distortion measurements. Significant variations in vehicle geometry included four configurations (three different sets plus a configuration with no generators) of vortex generators located aft of the vehicle cockpit.

This work represents the first known experimental inlet data set for a full vehicle configuration in a supersonic wind tunnel for a centerline top-mounted diverter-less bump inlet. Key results are noted in a number of areas. First, inlet recovery and distortion were insensitive to vehicle angle of attack, even when mounted in the aft location behind a vehicle canopy. Second, sideslip angles of 2° had a negative effect on inlet recovery when angle of attack was -2° ; however, recovery was largely unaffected by sideslip at

positive angle of attack. Third, inlet distortion values were affected by the presence of vortex generators, and by vehicle attitude and Mach number. Distortion data was collected with steady-state instrumentation. Further testing with dynamic pressure instrumentation, to obtain instantaneous distortion values, would better characterize the propulsion system operability. Distortion values need to be compared closely to engine requirements. Fourth, vortex generator design was important to maintain high inlet performance, where a long vortex generator configuration performed better than a short length design. The vortex generators appear to be critical to the performance of the centerline top-mounted inlet configuration. Finally, subsonic inlet performance demonstrated levels of recovery above 0.98 for most flight conditions. However, there was low recovery and high distortion at static conditions which may also be a concern for engine integration and these design challenges are being addressed in the current vehicle development program.

References

1. Norby, W.P., "Small Scale Inlet Testing for Low Cost Screening Applications," AIAA-90-1926, 1990 AIAA Joint Propulsion Conference, July 16-18, Orlando FL.
2. Soeder, R., "NASA Lewis 8- By 6-Foot Supersonic Wind Tunnel User Manual," NASA TM-105771, Feb. 1993.
3. SAE ARP1420C Gas Turbine Engine Inlet Flow Distortion Guidelines, Apr 2017.
4. Stephens, J., Hubbard, E., Walter, J., McElroy, T., "Uncertainty Analysis of the NASA Glenn 8×6 Supersonic Wind Tunnel," NASA CR—2016-219411, November 2016.
5. Arrington, A., "Calibration of the NASA Glenn 8- by 6-Foot Supersonic Wind Tunnel (1996 and 1997 Tests)," NASA/CR—2012-217270, January 2012.
6. Moore, M.T., "Distortion Data Analysis," AFAPL-TR-72-111, Feb 1973.

